UDC 539.4

Isothermal Fatigue and Creep-Fatigue Interaction Behavior of Nickel-Base Directionally Solidified Superalloy

A. U. Haq,[1] X. G. Yang, and D. Q. Shi

School of Energy and Power Engineering, Beihang University, Beijing, China

[1] amin_ulhaq@yahoo.com

The creep-fatigue interaction in directionally solidified nickel-base superalloy was analyzed with the modified Chaboche-based unified viscoplasticity constitutive model. The model features the anisotropic material behavior, hardening/ softening, and stress relaxation. Simple low-cyclic fatigue and specified hold time experiments were conducted on a directionally solidified superalloy (DZ125) at temperatures over 760°C. The material parameters were optimized considering its tensile, cyclic and creep behavior with the Levenberg–Marquardt optimization procedure. The model was constructed in FORTRAN and integrated in FEA software UMAT/ABAQUS. The results show that experimental and simulated hysteresis loop size/shape, peak stresses, stress relaxation, and related areas are closely matched. The modified constitutive model was found to be instrumental for revealing the fatigue and creep-fatigue interaction behavior of such materials and can be used for practical applications.

Keywords: fatigue, creep, creep-fatigue interaction, nickel-base superalloy.

Introduction. The severe operating environment in the hot section of the gas turbine engine, as well as the requirements of start-up and shutdowns, stimulate many time-dependent material damage mechanisms like fatigue, creep, creep-fatigue interaction, oxidation, and thermal-mechanical fatigue (TMF), which can cause a catastrophic failure. The safe and reliable design of these components requires a proper account of these complex mechanisms and a constitutive model to assess the stress-strain state (SSS) under various loading conditions. In the present study, the investigated material is a DZ125 nickel-base directionally solidified (DS) superalloy. Nickel-based DS superalloys are mainly used as engine blade materials due to their excellent high-temperature strength, and resistance to oxidation, fatigue, and creep [1–3]. The rationale behind the enhanced strength and excellent resistance is the addition of γ'-reinforced phase (Ni_3Al) into the γ-matrix and preferential directional solidification. This excludes the formation of grain boundary defects in the direction perpendicular to the applied stress and improves its creep resistance, but it also causes material anisotropy. Furthermore, the complex blade geometry with cooling channels and thermomechanical cyclic loading further complicate the design issue. The elevated temperature material behavior under fatigue [4, 5], creep-fatigue interaction [6, 7], and thermomechanical fatigue behavior [8, 9] remained the area of extensive research during the last few decades.

Two main approaches to characterize the time-dependent anisotropic behavior of material are the Crystal plasticity and phenomenological modeling. The former has the advantage of considering the physical phenomenon using slip system [10] but has the disadvantage of complexity as published by Li and Smith [11], while the later has successfully been used for polycrystalline material cyclic viscoplastic behavior [12]. The unified model of viscoplasticity one of the kinds of phenomenological model has been used and proposed by many researchers like Prager [13], Armstrong and Frederick [14] and further developed by Walker [15], Bodner and Parton [16], and Chaboche [17] for its simplicity in implementation. In phenomenological unified viscoplastic models, a group of internal state variables were introduced into the constitutive model to explain the hardening/ softening, relaxation and creep behavior; they are able to cover important mechanical/

thermal loading conditions; both fatigue and creep can be modeled simultaneously; material parameters can be easily optimized with isothermal monotonic experiments; and can be easily coded into the user material subroutine (UMAT).

To accurately model the fatigue-creep interaction of DZ125, simple low cycle fatigue (LCF) and dwell experiments have been conducted at 850 and 980°C. A transverse isotropic unified viscoplasticity model with the Chaboche-based framework and Ohno–Wang modification for material anisotropy and static recovery for stress relaxation is reformulated with two back stresses. The model is coded in UMAT using explicit integration methodology and implemented in ABAQUS. The parameters of the model are optimized using Lavenberg–Marquardt algorithm by grouping them into tensile, fatigue and creep behavior groups.

T a b l e 1

Chemical Composition of DS Superalloy DZ125 (wt.%)

Ni	Al	Ti	C	Cr	Co	B	Hf
Bal.	4.8–5.4	0.7–1.2	0.07–0.12	8.4–9.4	9.5–10.5	0.01–0.02	1.2–1.8
Mo	W	Ta	Fe	Si	Zr	S	P
1.5–2.5	6.5–7.5	3.5–4.1	≤ 0.30	≤ 0.15	≤ 0.08	≤ 0.01	≤ 0.01

1. Material Description and Experimental Methodology.

1.1. Test Material. DZ125, a directionally solidified nickel-based superalloy used in gas turbine blade application has the chemical composition shown in Table 1. Its semi-finished form is subjected to the following aging and heat-treatment procedure: 1180°C/3 h, 1230°C/3 h, AC+1100°C/4 h, and AC+870°C/20 h and AC (AC represent heat treatment with air cooling). DZ125 microstructure comprise the γ-matrix reinforced by γ'-reinforced phase which is uniformly distributed in the γ-matrix to improve the elevated temperature resistance of the material. The material is solidified in the longitudinal direction, which eliminates the transverse boundary slip. In the present paper, letters "L" and "T" denote longitudinal and transverse orientations, respectively.

1.2. Experimental Methodology. The strain-controlled LCF and creep-fatigue experiments are performed on a universal material testing system (WDW-50) and a 100 kN servo-hydraulic material tests system (MTS-810). The elevated temperature of 850 and 980°C are selected for the study of creep-fatigue interaction behavior. Test procedures GB/T 4338-2006 [18] and GB/T15248-2008 [19] are followed for tensile and fatigue tests respectively. The tensile tests are performed to investigate the influence of strain rate, orientation and temperature on the material stress-strain behavior and to optimize parameters related to the tensile behavior (not shown). In LCF testing, the strain range $\Delta\varepsilon = 1.6\%$, strain ratio $R_\varepsilon = -1$, and strain rate $\dot{\varepsilon} = 0.005$ mm/s were adopted to study the cyclic hardening/softening and mean stress relaxation behavior. To study the effect of dwell on LCF behavior of DZ125 at 850°C, isothermal LCF tests with strain ratio $R_\varepsilon = -1$, strain range $\Delta\varepsilon = 1.6\%$, and strain rate $\dot{\varepsilon} = 0.005$ mm/s, and dwell imposed at tensile peak were performed. Similarly, a strain range $\Delta\varepsilon = 1.2\%$ is applied at 980°C withhold applied at the peak of both tensile and compressive loadings. Hold times of 0, 30, 60, 120, and 300 s were employed. The testing temperature is controlled within ± 1.5°C over the fatigue specimen gauge length. An Epsilon-3448 extensometer was installed to measure the axial strain.

2. Unified Viscoplasticity Model. A unified viscoplasticity model using Chaboche framework is employed to study the creep-fatigue interaction behavior due to viscous effects active at elevated temperatures. The total strain rate comprised elastic and inelastic strain rates,

$$\dot{\varepsilon}_{ij} = \dot{\varepsilon}_{ij}^{\varepsilon} + \dot{\varepsilon}_{ij}^{in}. \tag{1}$$

The elastic portion of strain rate can be derived via the anisotropic theory

$$\dot{\varepsilon}_{ij}^{e} = C_{ijkl}\dot{\bar{\sigma}}_{kl}, \tag{2}$$

where C_{ijkl} is the anisotropic material compliance matrix. A viscoplastic potential of the Chaboche type $\Psi = \dfrac{K}{n+1}\left\langle \dfrac{F}{K} \right\rangle^{n+1}$ is employed. The McCauley bracket $\langle \cdot \rangle$ is the Heaviside function, operated as $\langle u \rangle = u$ if $u > 0$ and $\langle u \rangle = 0$ if $u \le 0$. The viscous parameter K controls the plastic flow and the parameter n controls the nonlinearity of the phenomenon. $F = J(\bar{S}'_{ij} - X'_{ij}) - R(p) - k_0$ is a yield function. Here, $\bar{S}'_{ij}$ and X'_{ij} are the deviatoric effective and back stress tensors components, respectively. The effective stress ($\tilde{\sigma}_{ij}$) relates stress (σ_{ij}) and creep damage (D) as $\tilde{\sigma}_{ij} = \sigma_{ij}/(1-D)$. The term $R(p)$ is the increase in yeild surface size, and k_0 a temperature-dependent initial yield stress. The von Mises yield criterion used is $J(\bar{S}'_{ij} - X'_{ij}) = \left[\dfrac{3}{2}(\bar{S}'_{ij} - X'_{ij})M_{ijkl}(\bar{S}'_{kl} - X'_{kl})\right]^{1/2}$; here J is the second invariant and M_{ijkl} is a fourth-order tensor used to describe DS-superalloy anisotropy. Now the modified viscoplastic flow rule can be expressed as

$$\dot{\varepsilon}_{ij}^{in} = \dot{p}\frac{\partial \Psi}{\partial \tilde{\sigma}} = \frac{3}{2}\left\langle \frac{J(\bar{S}'_{ij} - X'_{ij}) - R - k_0}{K} \right\rangle^{n} \frac{M_{ijkl}(\bar{S}'_{kl} - X'_{kl})}{J(\bar{S}'_{ij} - X'_{ij})}\frac{1}{1-D}. \tag{3}$$

Here $\dot{p}$ is the accumulated viscoplastic strain rate, which takes the following form:

$$\dot{p} = \sqrt{\frac{3}{2}\dot{\varepsilon}_{ij}^{in} M_{ijkl}^{-1}\dot{\varepsilon}_{kl}^{in}} = \left\langle \frac{F}{K} \right\rangle^{n}. \tag{4}$$

Equation (4) represents Norton's power law. Hardening describing kinematic, isotropic and thermal recovery are adopted here. The back stress evolution equation for nonlinear behavior with the Ohno–Wang modification is given as

$$X_{ij} = \sum\nolimits_{k=1}^{n} X_{ij}^{(k)}, \qquad k = 1, 2, \tag{5}$$

and

$$\dot{X}_{ij}^{(k)} = \frac{2}{3}c_k a_k \dot{\varepsilon}_{ij}^{in} - c_k \Phi(p)\left|\frac{J(X_{ij}^{(k)})}{a_k/\Phi(p)}\right|^{m_k} X_{ij}^{(k)}\dot{p} - \beta_k \left| J(X_{ij}^{(k)}) \right|^{r_k - 1} X_{ij}^{(k)}, \tag{6}$$

where $\Phi(p) = \Phi_s + (1-\Phi_s)e^{-\omega p}$, Φ_s and ω are the constitutive parameters, $C_k = c_k a_k$, c_k, a_k, β_k, m_k, and r_k are the material parameters. The first term in Eq. (6) is Prager's linear hardening, the second is the dynamic recovery which is also known as the Ohno–Wang modification, the third term is the static recovery. The isotropic hardening evolution is given as

$$\dot{R} = b(Q - R)\dot{p} + \gamma \left| Q_r - R \right|^{m-1}(Q_r - R), \tag{7}$$

where b, Q, γ, and m describe the deformation stimulated by the isotropic hardening. Q_r is asymptotic value of yield surface. Equation (7) first term expresses the cyclic hardening/

softening and second term is the rate dependent recoveries. For DZ125, the second term is not considered because the cyclic hardening gets steady in a few cycles, i.e., 20 cycles.

Since multiple damage mechanisms are active in the tertiary creep regime, hence evolutionary damage variable is introduced into the effective stress equation to simulate the tertiary creep strain. For simplicity, isotropic damage variable is introduced into the effective stress equation for longitudinal orientation only and the Kachanov–Rabotnov [20] law is used for capturing the tertiary creep regime. The Kachanov–Rabotnov creep damage law can be expressed as follows:

$$\dot{D} = \left[\frac{J(\tilde{\sigma}'_{ij})}{pa}\right]^{pr} (1-D)^{-pk}, \tag{8}$$

where $J(\tilde{\sigma}'_{ij})$ is the second invariant of effective stress and pa, pr, and pk are the temperature dependent material parameters determined from isothermal experimental creep fracture curves.

3. Parameters Optimization. The modified Chaboche model parameters can be identified using isothermal tensile, fatigue and creep experiments. The two groups of parameters at 850 and 980°C are optimized using the Levenberg–Marquardt algorithm, which produces accurate parameters and good convergence speed by iteratively minimizing the relative deviation between experimental and simulated results till the root mean square of the relative deviation is less than the specified limit. Fatigue and creep damages are related to their respective inelastic strain accumulated over a period of time, whereas inelastic behavior in tension is a short time phenomenon. Therefore, the material parameters related to them can be grouped into tensile, cyclic hardening/softening and creep behavior. Parameters are optimized as follows: Elastic region of different orientations tensile curves were used to calculate E_{11}, E_{33}, and E_{23}; μ_{11} and μ_{23} were acquired using material manual. Parameters K, n, k_0, a_1, a_2, c_1, and c_2 are identified based on the inelastic region of the tensile curves; M_{11}, M_{33}, and M_{55} are initially preset as unity. In this case, experimental results for both longitudinal and transverse orientations were incorporated into the optimization algorithm, and parameters were obtained by the curve fitting. Material parameters related to cyclic hardening/softening m_1, m_2, Φ_s, and ω were optimized by fitting of the completely reversed ($R_\varepsilon = -1$) isothermal fatigue test continuous cyclic stress range data. The parameters related to isotropic hardening b and Q were optimized by fitting of the isothermal fatigue test $R_\varepsilon = 0$ continuous cycles mean stress relaxation data. Once all of the above parameters have been acquired at the first iteration, the procedure was repeated while keeping the exponential parameters (i.e., n, m_1, m_2, and ω) unchanged, in order to finally optimize the remaining parameters related to the tensile and cyclic hardening/softening and mean stress relaxation behavior. Finally, the parameters related to the creep and creep damage γ_1, γ_2, β_1, β_2, pa, pr, and pk were optimized by curve fitting the creep and rupture strength data at different stresses corresponding to each temperature.

4. Results and Discussion. Strain-controlled symmetric/asymmetric fatigue tests are usually applied to characterize the material hardening/softening and stress relaxation behavior. In addition to the cyclic fatigue behavior, the creep-fatigue interaction behavior is also very important for the damage analysis of hot section components. The Chaboche based unified constitutive model has the capability of simulating across the two areas (i.e., fatigue and creep). The capability of the modified Chaboche model for simulating a variety of responses in longitudinal and transverse orientations and at different strain ranges has been thoroughly evaluated against uniaxial experiments, which comprised strain-controlled fatigue and creep-fatigue interaction tests and stress-controlled creep ones. However, the analysis of fatigue and creep-fatigue interaction behavior at elevated temperatures of 850 and 980°C was applied in the present research to observe the material behavior and display the simulating capability of the modified Chaboche model.

4.1. Hysteresis Loop Features/Characteristics. Hysteresis loop represents the elastic-viscoplastic energy/work per cycle for an elastic-viscoplastic material. This parameter can be used as a damage indicator for the quantification of LCF damage which accumulates as a viscoplastic work. Hysteresis loop of DZ125 at different temperatures and strain range, in longitudinal/transverse orientation for symmetric strain cycling show different stress evolution behavior. The LCF experimental and simulated first hysteresis loop comparison in longitudinal and transverse orientation for 850 and 980℃ at strain rate 0.005 mm/s, strain range of 1.6%, and strain ratio $R = -1$ are shown in Fig. 1. The simulated hysteresis loop area and shape are in good agreement with the experimental results. The strain hardening and dynamic recovery terms in the back stress equation basically dictate the model to accurately capture the size and shape of the hysteresis loop.

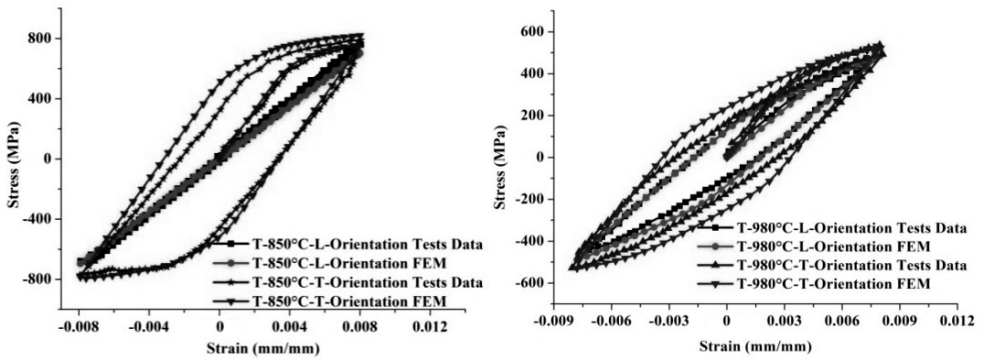

a b

Fig. 1. DZ125 cyclic behavior at strain ratio $R = -1$, $\dot{\varepsilon} = 0.005$ mm/s, and $\Delta\varepsilon = 1.6\%$ at 850 (a) and 980℃ (b).

In addition, the maximum and minimum stresses, which are related to the isotropic hardening (i.e., increase/decrease of yield surface, R) are well simulated by the model as shown in Fig. 1. The hysteresis loops area, which represents the elastic-viscoplastic energy, reveals that the energy dissipated during one cycle in transverse orientation is greater than the longitudinal orientation (i.e., blade axis) under the same loading condition. This implies that DZ125 strength is high along the blade axis, which proves the goal of directional solidification to withstand high stresses. At high-temperatures, DZ125 shows less anisotropic behavior as depicted in Fig. 1b at 980℃, where the hysteresis loops in the longitudinal and transverse directions become similar. This implies that the dislocation distribution at elevated temperatures is homogeneous, which also results in the reduced stresses at 980 than 850℃ (i.e., the material is softened). The material homogeneity can be quantified by the ratio of longitudinal/transverse hysteresis loop areas. The hysteresis loop area is a product of stress (in MPa) and strain (in %), which is calculated by the original integration analysis tool. Assuming that, in case of a fully homogeneous behavior, the area ratio is equal to unity, the homogeneous behavior of CDZ125 at 980° corresponds to the area ratio of 60.25% [i.e., $(0.6025/1)\times 100 = 60.25\%$], as compared to that of 3.63% at 850℃.

Moreover, DZ125 hardening/softening behavior can be characterized by the stress response against the number of cycles in the longitudinal orientation, where centrifugal stresses will be high. The experimental hardening/softening behavior of DZ125 at 850 and 980℃ in the longitudinal orientation is shown in Fig. 2. At lower temperature of 650℃ DZ125 shows a continuous cyclic hardening with no stabilization (not shown). At 850℃, DZ125 exhibits a cyclic hardening followed by softening. The hardening behavior is more prominent in the higher strain range, while continuous softening is observed within lower

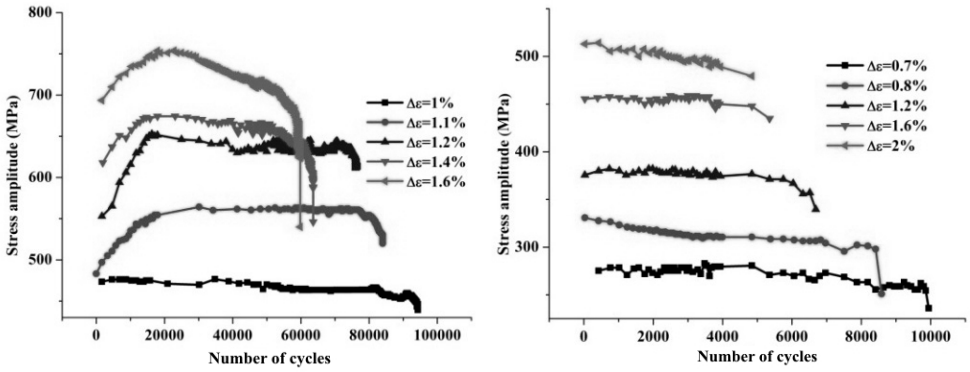

Fig. 2. DZ125 stress evolution behavior along the L orientation ($\dot{\varepsilon} = 0.005$ mm/s, $R_\varepsilon = -1$) at 850 (a) and 980℃ (b).

strain ranges. At a high temperature of 980℃, DZ125 shows a continuous cyclic softening for all strain ranges. In short, DZ125 exhibits both strain range- and temperature-dependant behavior.

4.2. Hold Effect. Introducing hold into the LCF strain-controlled experiments produces stress relaxation, which is also referred to as creep-fatigue interaction [6, 7]. This phenomenon is explored in for complex TMF experiments where the temperature also fluctuates along with the strain cycling. The effect of viscosity is obtained from the inelastic deformation produced during the hold time of creep-fatigue test, and its modeling is vital for damage analysis during creep-fatigue interaction [21]. This effect is associated with the time-recovery, which corresponds to the re-establishment of a crystalline structure.

On the one hand, the stress relaxation is expected to be directly linked to the hold time; however, this can also be observed during the cyclic deformation in LCF experiments as in Fig. 2a and 2b. In the present research, the influence of tensile/ compressive hold on the LCF deformation behavior of DZ125 was investigated. LCF fatigue experiments with 0, 60, 120, and 300 s holds were conducted to characterize the behavior of DZ125 with the strain range of 1.6% and strain rate of 0.005 mm/s at 850℃, as well as the strain range of 1.2% and strain rate of 0.005 mm/s at 980℃, respectively.

The peak stress evolution behavior of material with cycles is the macroscopic representation of microstructural changes taking place in the material. DZ125 undergoes a hardening evolution with cycles at zero holds as shown in Fig. 3a, but exhibits a softening behavior with the introduction of the tensile hold. The influence of hold on LCF behavior of DZ125 is depicted in Fig. 3a, where long hold times cause the increased stress relaxation and subsequent deterioration of low-cycle fatigue life. It can also be observed from the experimental data that DZ125 exhibits a similar relaxation behavior at tensile hold of 120 and 300 s. The comparison of the 10th hysteresis loop for creep-fatigue experiments at different hold times is shown in Fig. 3b. The larger hysteresis loop area with a hold manifests the increased damage accumulation in DZ125 with a hold. Furthermore, DZ125 produces similar hysteresis loop shapes for different dwell times of creep-fatigue experiments.

The creep-fatigue simulation and experimental results at 850 and 980℃ are presented in Fig. 4. In our model, the stress relaxation during holding is dictated by the flow rule and static recovery terms of the model. The Norton's flow rule is employed in the constitutive model, where the viscous parameter K controls the plastic flow and the parameter n controls the nonlinearity of the phenomenon. The hysteresis loop size, shape, peak stresses

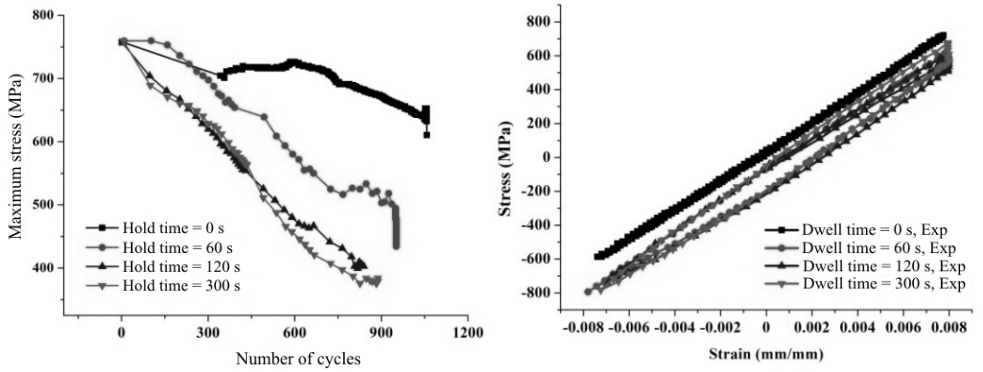

a b

Fig. 3. Dwell experiments at 850℃, $\dot{\varepsilon} = 0.005$ mm/s, and $\Delta\varepsilon = 1.6\%$: (a) stress evolution; (b) hysteresis loop.

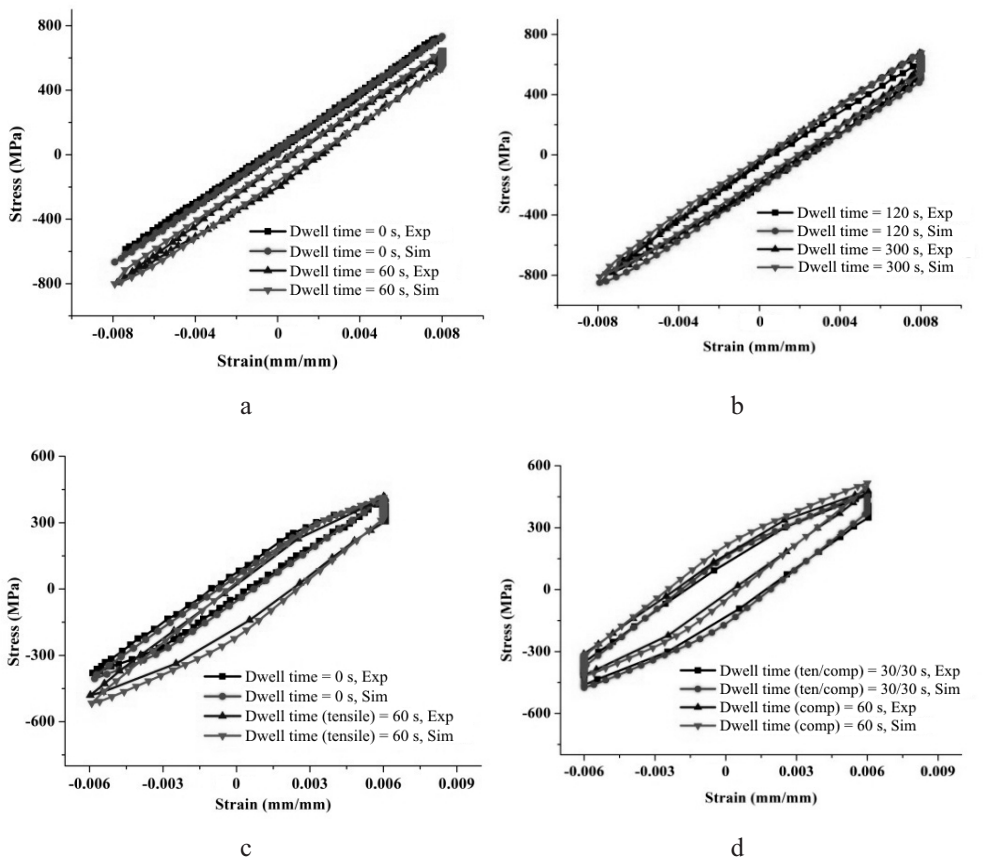

a b

c d

Fig. 4. Comparison of cyclic hold behavior with $\dot{\varepsilon} = 0.005$ mm/s and different hold times [(a), (b) $T = 850$℃, $\Delta\varepsilon = 1.6\%$; (c), (d) $T = 980$℃, $\Delta\varepsilon = 1.2\%$].

and relaxed stress during hold are in good agreement with the experimental results which validate the model capability for creep-fatigue interaction behavior. Based on the hysteresis loop areas, the increase in the ratio of experimental (simulated) hold area to zero hold area

from 4.379 (4.367) at 60 s hold to 6.07 (5.6) at 120 s hold and 5.86 (5.9) at 300 s hold reveals that the creep damage per cycle increases with the hold time until 120 s at 850℃ is reached where the cyclic peak stress behavior and hysteresis loop areas becomes similar to 300 s tensile hold behavior as depicted in Fig. 3. At 980℃, the compressive hold further aid the damage process as depicted by an increase in the hysteresis loop area in Fig. 4d.

Conclusions. Based on the results obtained, the following conclusions are made:

1. Fatigue tests of DZ125 exhibit strong temperature and orientation effects on the stress-strain response. The hysteresis loop area of 826.69 corresponding to 850℃ and the transverse orientation exceeds that of the longitudinal orientation (equal to 30.37). This implies that the strength of DZ125 is higher along the longitudinal orientation. Furthermore, the area ratio of longitudinal to transverse hysteresis loop, which quantifies the material homogeneity, is 0.6025 at 980℃, which implies that the material behavior in longitudinal and transverse orientations is homogeneous by 60.25% (i.e., the material behavior is getting more homogeneous with temperature).

2. The introduction of hold causes the increased stress relaxation and consequently results in the degradation of the low-cycle fatigue life. The increase of a hysteresis loop area with the hold manifests the increased damage accumulation under creep-fatigue conditions. A similar stress relaxation behavior was observed at 120 and 300 s tensile hold times. This behavior may represent the saturation effect or implies that the hold time too short to cause any creep damage. The area ratio of hysteresis loop with combined 30/30 s tensile/compressive holds to that without hold is equal to 2.617, whereas those for a single 60 s tensile and compressive holds to that without hold are 1.87 and 1.857, respectively. This implies that the combined tensile and compressive hold is more damaging than a single tensile or compressive hold of equal time under creep-fatigue interaction conditionst. Based on the experimental and simulated area ratio, damage per cycle from a single tensile and a single compressive holds of 60 s, as compared to that with a combined hold of 30/30 s, is increased by 28.5 and 29.76%, respectively.

3. The model parameters were optimized by associating them with tensile, cyclic and creep contributions, respectively, via the Lavenberg–Marquardt algorithm. The simulation results are in good agreement with experimental results, which proves the optimization procedure reliability.

4. The modified Chaboche-based unified constitutive model properly describes the low-cycle fatigue and creep-fatigue interaction behavior of DZ125.

1. R. A. Kupkovits and R. W. Neu, “Thermomechanical fatigue of a directionally-solidified Ni-base superalloy: Smooth and cylindrically-notched specimens,” *Int. J. Fatigue*, **32**, No. 8, 1330–1342 (2010).
2. M. M. Shenoy, D. L. McDowell, and R. W. Neu, “Transversely isotropic viscoplasticity model for a directionally solidified Ni-base superalloy,” *Int. J. Plasticity*, **22**, No. 12, 2301–2326 (2006).
3. D. Shi, C. Dong, X. Yang, et al., “Creep and fatigue lifetime analysis of directionally solidified superalloy and its brazed joints based on continuum damage mechanics at elevated temperature,” *Mater. Design*, **45**, 643–652 (2013).
4. M. G. Fahrmann and S. K. Srivastava, “Low cycle fatigue behaviour of HAYNES 230 alloy,” *Mater. High Temp.*, **31**, No. 3, 221–225 (2014).
5. P. Li, Q. Q. Li, T. Jin, et al., “Comparison of low-cycle fatigue behaviors between two nickel-based single-crystal superalloys,” *Int. J. Fatigue*, **63**, 137–144 (2014).
6. R. Ahmed, P. R. Barrett, and T. Hassan, “Unified viscoplasticity modeling for isothermal low-cycle fatigue and fatigue-creep stress–strain responses of Haynes 230,” *Int. J. Solids Struct.*, **88–89**, 131–145 (2016).

7. Y. Tian, D. Yu, Z. Zhao, et al., "Low cycle fatigue and creep–fatigue interaction behaviour of 2.25Cr1MoV steel at elevated temperature," *Mater. High Temp.*, **33**, No. 1, 75–84 (2016).
8. M. M. Shenoy, A. P. Gordon, D. L. McDowell, and R. W. Neu, "Thermomechanical fatigue behavior of a directionally solidified Ni-base superalloy," *J. Eng. Mater. Technol.*, **127**, No. 3, 325–336 (2005).
9. P. Zhang, Q. Zhu, G. Chen, and C. Wang, "Review on thermo-mechanical fatigue behavior of nickel-base superalloys," Mater. Trans., 56, No. 12, 1930–1939 (2015).
10. C. L. Xie and E. Nakamachi, "Investigations of the formability of BCC steel sheets by using crystalline plasticity finite element analysis," *Mater. Design*, **23**, No. 1, 59–68 (2002).
11. S. X. Li and D. J. Smith, "Development of an anisotropic constitutive model for single-crystal superalloy for combined fatigue and creep loading," *Int. J. Mech. Sci*., **40**, No. 10, 937–948 (1998).
12. J. L. Chaboche, "Constitutive equations for cyclic plasticity and cyclic viscoplasticity," *Int. J. Plasticity*, **5**, No. 3, 247–302 (1989).
13. W. Prager, "A new method of analyzing stresses and strains in work-hardening plastic solids," *J. Appl. Mech.*, **23**, 493–496 (1956).
14. P. J. Armstrong and C. O. Frederick, *A Mathematical Representation of the Multiaxial Bauschinger Effect*," CEBG Report RD/B/N 731, Central Electricity Generating Board and Berkeley Nuclear Laboratories, Research & Development Department (1966).
15. K. P. Walker, *Research and Development Program for Non-Linear Structural Modeling with Advanced Time-Temperature Dependent Constitutive Relationships*, Technical Report NASA-CR-165533, PWA-5700-50 (1981).
16. S. R. Bodner and Y. Partom, "Constitutive equations for elastic-viscoplastic strain-hardening materials," *J. Appl. Mech.*, **42**, No. 2, 385–389 (1975).
17. J. L. Chaboche, "A review of some plasticity and viscoplasticity constitutive theories," *Int. J. Plasticity*, **24**, No. 10, 1642–1693 (2008).
18. *GB/T 4338: 2006. Metallic Materials – Tensile Testing at Elevated Temperature*, Chinese Standard. Implemented on January 1, 2007.
19. *GB/T 15248: 2008. The Test Method for Axial Loading Constant-Amplitude Low-Cycle Fatigue of Metallic Materials*, Chinese Standard. Implemented on October 1, 2008.
20. J. L. Chaboche, A. Gaubert, P. Kanouté, et al., "Viscoplastic constitutive equations of combustion chamber materials including cyclic hardening and dynamic strain aging," *Int. J. Plasticity*, **46**, 1–22 (2013).
21. J. L. Chaboche, "Continuum damage mechanics: Part II – Damage growth, crack initiation, and crack growth," *J. Appl. Mech.*, **55**, No. 1, 65–72 (1988).

Received 15. 09. 2017